Photodissociation of NH_2 in the Two-Dimensional Light−Heavy−Light Approximation

A. Koch

H. C. Ørsted Institute, Chemical Laboratory III, Universitetsparken 5, DK-2100 Copenhagen Ø, Denmark

Received: October 1, 1996; In Final Form: December 4, 1996[⊗]

Photodissociation dynamics through the $3^2A'(2^2A_1)$, the $2^2A''(2^2B_1)$, and the $3^2A''(1^2A_2)$ states of NH_2 are studied in the two-dimensional light−heavy−light approximation at the equilibrium angle of the ground state. The NH_2 radical is of relevance in the chemistry of interstellar clouds and cometary atmospheres. Photodissociation is the major destruction mechanism of the radical in these environments. Since it is difficult to produce the molecule in the laboratory, little is known about this process from experiments. Total and vibrationally resolved partial cross sections have been calculated. The surfaces of the transition dipole moments are taken into account in all calculations. By far the largest total cross section of photodissociation is found for the $2^2A''(2^2B_1)$ state. Through the bound $3^2A'$ (2^2A_1) state, photodissociation mainly proceeds through resonant levels close to the dissociation limit, corresponding to coupled antisymmetric−symmetric stretching motions. The Fourier transform of the autocorrelation function also contains a number of bound vibrational levels, which are assigned to the antisymmetric and coupled antisymmetric−symmetric stretching vibrational levels. Since the $3^2A'(2^2A_1)$ state has the same equilibrium bond angle as the X^2B_1 ground state, the present calculations are expected to give the essential physical properties of the photodissociation dynamics through this state. Direct photodissociation proceeds through the $3^2A''(1^2A_2)$ state. By far the largest cross section of photodissociation is found for the $2^2A''(2^2B_1)$ state. The results from this work are compared to an experimental fragment fluorescence spectrum from the literature.

1. Introduction

The NH_2 radical is widely observed in cometary atmospheres[1] and is thought to be an important link in the nitrogen chemistry in interstellar clouds.

The relevance of the NH_2 radical for astrophysics results from its property as an indicator for the production pathways of nitrogen-bearing molecules.[2] The NH_2/NH_3 ratio is supposed to clarify whether NH_3 is preferentially formed by gas phase reactions or on grains.

The most usual formation path of NH_2 in the gas phase of interstellar clouds is through the reaction of N^+ ions, which are mainly formed by cosmic ray ionization, with H_2.[3] By further abstraction reactions with H_2 and subsequent recombination with free electrons, further NH_x ($x \geq 3$) species can be formed. In the presence of sufficiently high UV photon fluxes, NH_2 is also produced via photodissociation of NH_3. In turbulent clouds NH_2 can also be formed via subsequent abstraction reactions of H_2 with N. Since the reaction barriers of these processes are high, shock speeds as high as 25−40 km s^{-1} are required to render this production pathway efficient.[4] Collisions of the released H atoms with NH_3 allow destruction of NH_3 to yield NH_2 again. The primary destruction route of NH_2 as well as NH_3 in so-called photon-dominated regions (PDRs,[5]) is photodissociation, which, however, becomes less efficient at higher depth into the interstellar cloud due to the shielding of the radiation field by the outer layers.[2]

Crucial information for the determination of the NH_2 column density from observations and chemical reaction network models is the photodissociation rate, which is a convolution of the photodissociation cross section and the interstellar radiation field, both as functions of the excitation energy. However, little is known about photodissociation of NH_2 from experiments, since the radical is difficult to produce in the laboratory. On the other hand, it is small enough for accurate quantum chemical ab initio calculations.

In this study photodissociation processes of NH_2 through various low-lying excited states are studied. The photodissociation dynamics calculations are based on ab initio multireference configuration interaction (CI) calculations from ref 6 employing the MRD-CI method.[7−10] Such calculations provide potential energy surfaces (PESs) for the ground state and the excited states and the transition dipole moments connecting them. The subsequent solution of the Schrödinger equation for nuclear motion using these PESs enables a quantitative determination of the total and partial photodissociation cross sections. In the low-temperature interstellar medium the transitions from the bound ground state to dissociative excited states are mainly limited to those from the zeroth vibrational level of the ground state. Therefore the present work is restricted to these transitions.

The NH_2 radical has C_{2v} symmetry in its X^2B_1 ground state. The equilibrium geometry according to ref 6 is $r_1 = r_2 = 1.954$ a_0 and $\alpha_{eq} = 102.4°$. This is similar to the older experimentally determined ground state equilibrium geometry[11] with $r_1 = r_2 = 1.935\ 08\ a_0$ and $\alpha_{eq} = 103°$. The ground state is bound with a relatively low dissociation energy of 3.93 eV in accordance with the radical properties. Previous theoretical studies of NH_2 (e.g. refs 12 and 13) mainly focused on the avoided crossing between the low-lying A^2A_1 and B^2B_2 states (here in the notation of the C_{2v} symmetry group of the X^2B_1 ground state), which both become $^2A'$ states in C_s symmetry, and on the low-lying states of NH^+. The X^2B_1, A^2A_1, and B^2B_2 states, which are the lowest ones at the ground state equilibrium geometry, are pure valence-type states at all bond distances. The 2^2B_1 and the 2^2A_1 states are also valence states at the ground state equilibrium geometry. All higher-lying states are predominantly Rydberg in character at the ground state equilibrium geometry. Rydberg-valence interactions occur in the potentials of the 2^2B_1, 2^2A_1, and 1^2A_2 states. A previous MCSCF study of potential energy curves, transition dipole moments of the five lowest doublet states along one NH bond length (with the second one

[⊗] Abstract published in *Advance ACS Abstracts,* February 1, 1997.

S1089-5639(96)03020-4 CCC: $14.00

fixed at the ground state equilibrium value), and a calculation of the cross sections of photodissociation through the 2 and $3^2A'$ states into NH + H in a one-dimensional (1D) approximation have been undertaken by Saxon et al.[14] While two broad resonances with low peak intensities of 2.7 and 4.3 $\times$ 10^{-21} cm^2 are found for the $2^2A'$ state in accordance with its bound state character, the cross section through the $3^2A'$ state, which is also bound with respect to photodissociation but has a relatively small dissociation energy of 0.56 eV, has a high maximum of 2.9 $\times$ 10^{-17} cm^2 with a width of 0.042 eV at 7.64 eV and a lower ($\sim$3 $\times$ 10^{-19} cm^2) and broader one at 8.26 eV. In spite of the bound state character of the $3^2A'$ state, the high threshold resonance occurring in the 1D treatment made this state appear to be a promising candidate for photodissociation of the radical under interstellar conditions. The resonance structure found in this 1D approximation is expected to be altered considerably, if the second N−H bond length is also varied.

More recently MC-CEPA calculations of the vertical and adiabatic ionization energies and of the potential energies of the ground state and eight low-lying excited states along the bending coordinate at constant $r_1 = r_2 = 1.954\ a_0$ have been performed by Biehl et al.[15] From their calculations the equilibrium bond angles of the three states at constant r_1, r_2 equal to the ground state equilibrium bond lengths are known. For the $3^2A'(2^2A_1)$ state an equilibrium bond angle of 105.0° is found,[15] which is 2.6° above the ground state equilibrium bond angle. The comparison of the potential curves from ref 15 along the bond angle at constant $r_1 = r_2 = r_{eq}$ for the 2^2A_1 and the X^2B_1 states shows that not only the minima of the curves but also the derivatives around the minima are in good accordance. Therefore a 2D treatment of the photodissociation dynamics with the bond angle fixed at the ground state equilibrium angle can be expected to be a good approximation to the full 3D calculation for this state. A 2D approximation has also been chosen for the A^1B_1 state of H_2O with an equilibrium bond angle similar to that in the ground state.[16]

For the other two dissociative excited states considered here, $2^2A''(2^2B_1)$ and $3^2A''(1^2A_2)$, an equilibrium angle of 180° has been found.[6,15] Therefore the present 2D results have to be scrutinized by subsequent 3D calculations for both of these states. However, the total cross sections integrated over excitation energy (or photon wavelength), which are crucial quantities in astrochemical applications of molecular dynamics, are expected to be accurate within 15%. Since the ground state vibrational wave function is normalized, deviations between the 2D and 3D results for the integrated total cross sections can only result from non-Franck−Condon effects involving the bending motion.

The 2D results are also helpful for the understanding of a recent experimental fragment fluorescence spectrum[15] for the $NH(A^3\Pi)$ + H asymptote. In this experiment NH_2 is photolyzed in a flow system with tunable synchrotron radiation from 200 to 105 nm and other vacuum ultraviolet light sources. In previous work on the formation of $NH(A^3\Pi)$ in the photolysis of hot NH_2 at 193 nm (6.42 eV), Kenner et al.[17] concluded that the absorption of NH_2 at this wavelength is due to the transition from rotationally excited levels of the X^2B_1 ground state of NH_2 to the 2^2A_1 state. The observed polarization of the $NH(A^3\Pi \rightarrow X^3\Sigma^-)$ fluorescence was attributed to high overtones of the out−off plane rotation in the initial X^2B_1 state and a subsequent fast dissociation via the 2^2A_1 state of NH_2. This course of the fragmentation process would lead to the observed preferential population of the antisymmetric Λ doublets of $NH(A^3\Pi)$; i.e. the singly occupied π orbital oriented perpendicular to the molecular plane of NH_2 is assumed to couple to the corresponding rotational angular momentum (i.e. the rotational momentum perpendicular to the molecular plane).[17]

A comparison of our results with recent spectroscopical data will follow in section 4.4 of this study. The importance of the 2^2A_1 state for photodissociation of NH_2 will be discussed in sections 4.1 and 5. The following section summarizes some information from the electronic structure calculations[6] which is essential for the understanding of the photodissociation dynamics through the $3^2A'(2^2A_1)$, $2^1A''(2^2B_1)$, and $3^2A''(1^2A_2)$ states (from here the C_s notation of the states will be used throughout the text). Section 3 reviews the method of the dynamics calculations and important details of the calculation procedure. In Section 4 the results for the calculated cross sections of photodissociation will be presented and discussed, including a comparison with recent experimental results. Conclusions will follow in Section 5.

2. Information from Electronic Structure Calculations

The ab initio potential energy surfaces (PESs) and transition dipole moments from ref 6, which enter the dynamics calculations, have been computed by means of the MRD-CI package including a configuration selection and energy extrapolation procedure[7−10] and on the basis of $^4A''$ molecular orbital functions from a Roothaan-HF-SCF procedure.

Further details of the method and performance of the electronic structure calculations are given in ref 6. Both N−H bond lengths have been varied independently in C_s symmetry in the calculations, whereas the bond angle is kept fixed at the value of the ground state equilibrium bond angle for each of the three excited states under consideration.

The coordinate system has been chosen such that $\hat{x}$ is perpendicular to the molecular plane and that the C_2 axis of the molecule is parallel to $\hat{z}$. In C_{2v} symmetry the *z*-component of the electric transition dipole moment lies in the A_1 representation, the *y*-component in B_2, and the *x* component in B_1. In C_s symmetry the *y*- and *z*-components of the transition dipole moment lie both in A′, whereas *x* lies in A″.

In the present work spline fit interpolations along the r_1 and r_2 internal coordinates have been used in order to represent the ab initio potentials for the X^2A'' ground state and the $3^2A'$, the $2^2A''$, and $3^2A''$ excited states on a dense and regular grid. All PESs are symmetric with respect −3to the $r_1 = r_2$ line. The ground state PES (Figure 1) has a minimum of −3.99 eV with respect to the dissociation limit at $r_1 = r_2 = 1.954\ a_0$.

The $3^2A'$ PES has two identical shallow minima at $r_1 = 2.020\ a_0$ and $r_2 = 2.881\ a_0$ symmetric to the $r_1 = r_2$ line (Figure 2). The potential energy at the minima is 7.22 eV, 0.32 eV below that at the ground state equilibrium geometry. The lowest asymptotic energy of +0.56 eV with respect to the minima of the PES is found parallel to the $r_{1,2}$ axes, keeping the second bond distance fixed at 1.98 a_0. Since the vertical excitation energy is lower than the minimum asymptotic energy by 0.25 eV, the total cross section of photodissociation through this state is expected to be much smaller than that through the $2^2A''$ state. Due to configuration interaction with an antibonding valence-type state, a small potential well arises parallel to the r_1 and r_2 axes, between r_2 (r_1) = 3.5 and 4.5 a_0. This well is highest, i.e. 3.15 eV with respect to the minimum of the PES, on the $r_1 = r_2$ line around 4.3 a_0 and decreases to zero in the asymptotic range of the PES. A nodal line on the surface of the electric transition dipole moment around 3 a_0, which had already been discovered by Saxon et al.[14] in the 1D approximation at one N−H bond length fixed at that of the ground state equilibrium (eq.) geometry, also reveals this configuration interaction.

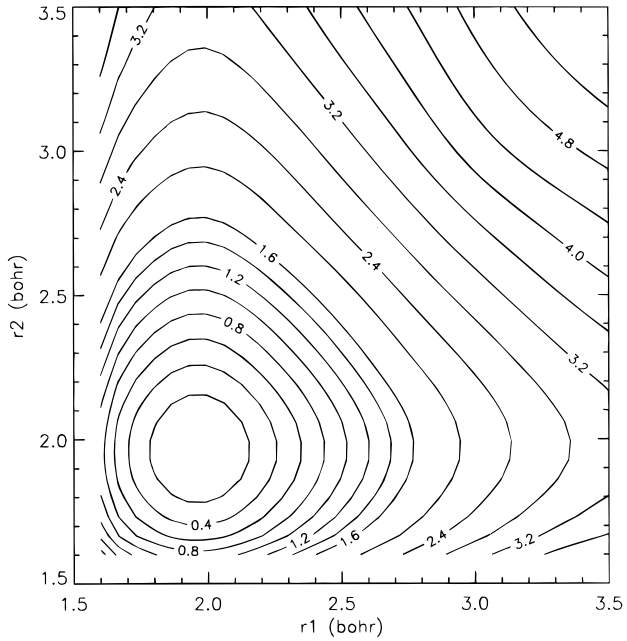

Figure 1. Two-dimensional contour plot of the potential energy surface of the X^2A'' ground state of NH_2 at the eq. bond angle of 102.4° as a function of the internal coordinates (r_1, r_2). The numbers at the contour levels denote the potential with respect to the minimum of this state in eV. The ground state eq. geometry is at $r_1 = r_2 = 1.954\ a_0$.

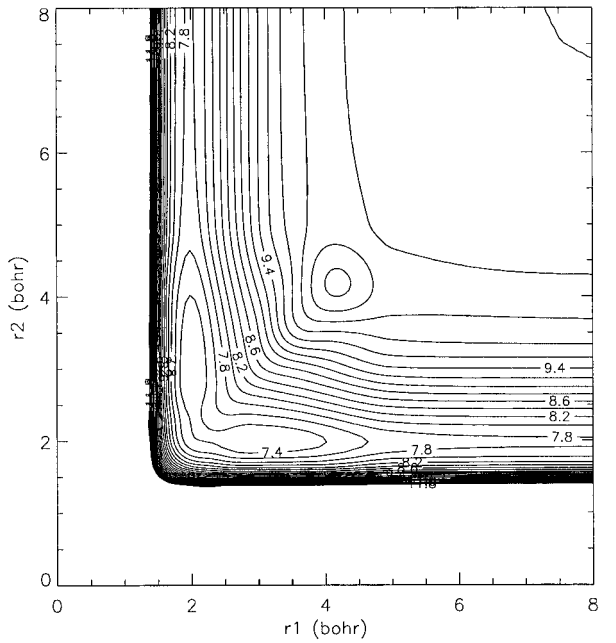

Figure 2. Two-dimensional contour plot of the potential energy surface of the $3^2A'$ state of NH_2 at the ground state eq. bond angle of 102.4° as a function of the internal coordinates (r_1, r_2). The numbers at the contour levels denote the potential of the excited state with respect to the minimum of the electronic ground state in eV. The ground state eq. geometry is at $r_1 = r_2 = 1.954\ a_0$.

However, this nodal line is outside the Franck−Condon region and does therefore not affect the photodissociation dynamics through this state significantly. At the ground state eq. geometry the transition dipole moment is 0.410 au.[6] Figure 3 shows the shape of the transition dipole moment inside the Franck−Condon region, i.e. in the bond lengths range from 1.67 to 2.23 a_0. In this range the transition dipole moment changes its value only weakly. A minimum of the PES with respect to the symmetric stretching coordinate of the ground state exists at an energy of 7.37 eV along the $r_1 = r_2$ line at 2.12 a_0. This

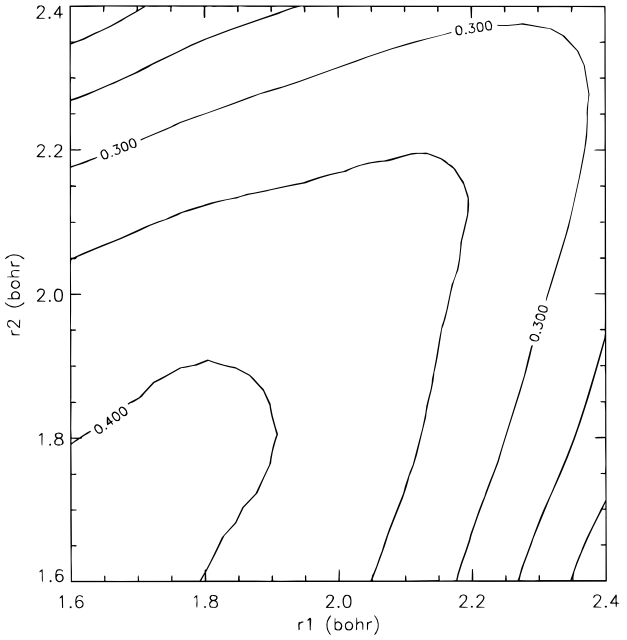

Figure 3. Two-dimensional contour plot of the geometry-dependent dipole transition moment $3^2A' \leftarrow X^2A''$ in au at the ground state eq. bond angle of 102.4° as a function of the internal coordinates (r_1, r_2). The numbers at the contour levels denote the electric dipole transition moment in au. The ground state eq. geometry is at $r_1 = r_2 = 1.954\ a_0$.

minimum is lower than the energy at the ground state equilibrium geometry by 0.16 eV, which correspond to the minimum height of the barrier between the two indistinguishable troughs. With respect to the 2D PES the minimum along the $r_1 = r_2$ line is a saddle point. These results are in accordance with the previous 1D results by Saxon et al.[14] along one N−H bond length. In their treatment the $3^2A'$ state has a saddle point at an N−H bond length slightly larger than the ground state equilibrium bond length of 1.954 a_0 and a shallow minimum around 3.0 a_0.

Because of the particular shape of the PES with two identical minima symmetrical to the $r_1 = r_2$ line and the minimum along $r_1 = r_2$, at which the minimum barrier between the two potential troughs occurs, a complicated pattern of anharmonic vibrational modes has to be expected for this PES. As a first indication for the ratios of the frequencies and the way in which photodissociation proceeds, it is instructive to compare the directional derivatives at particular points of the PES. At the two minima of the PES, the derivative of the PES along the longer symmetry axis of each of the two potential troughs is smaller by a factor of 4 than that perpendicular to this direction. The latter one is smaller by a factor 1.5 than that at the minimum along the $r_1 = r_2$ line. At the ground state eq. geometry, the derivatives along the $r_1 = r_2$ line and along each of the coordinate axes $r_{1,2}$ are essentially the same. Therefore a large part of the flux will be trapped in the bound region of the potential, even at excitation energies above the dissociation limit, and resonant photodissociation will account for most of the total and partial cross sections.

The $2^2A''$ PES has a local minimum at $r_1 = r_2 = 2.03\ a_0$, i.e. close to the ground state equilibrium geometry (Figure 4). The height of the barrier to dissociation into the two low-lying identical $NH(a^1\Delta) + H$ asymptotes is 0.15 eV. It can be expected that the barrier to dissociation strongly affects the photodissociation dynamics through this state. The transition dipole moment at the ground state equilibrium geometry is 0.607 au (*z*-component). This indicates that the total cross section of photodissociation through this state will be large compared with

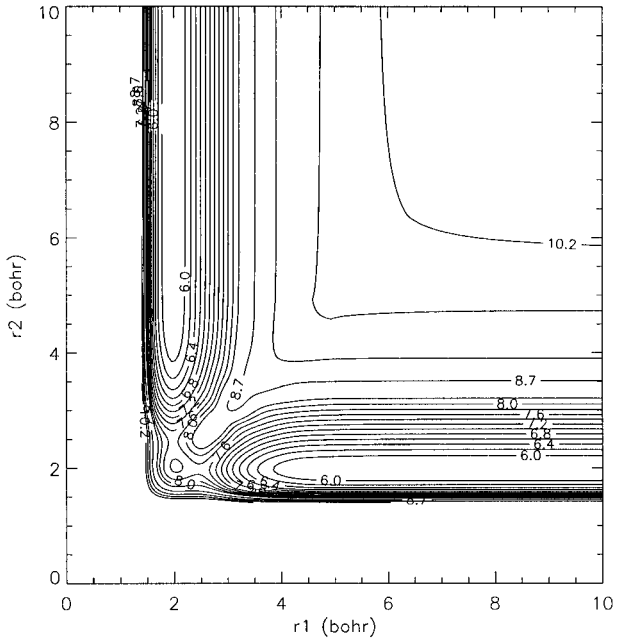

Figure 4. Two-dimensional contour plot of the potential energy surface of the $2^2A''$ state of NH_2 at the ground state eq. bond angle of 102.4° as a function of the internal coordinates (r_1,r_2). The ground state eq. geometry is at $r_1 = r_2 = 1.954$ a_0. Contour levels as indicated in Figure 2.

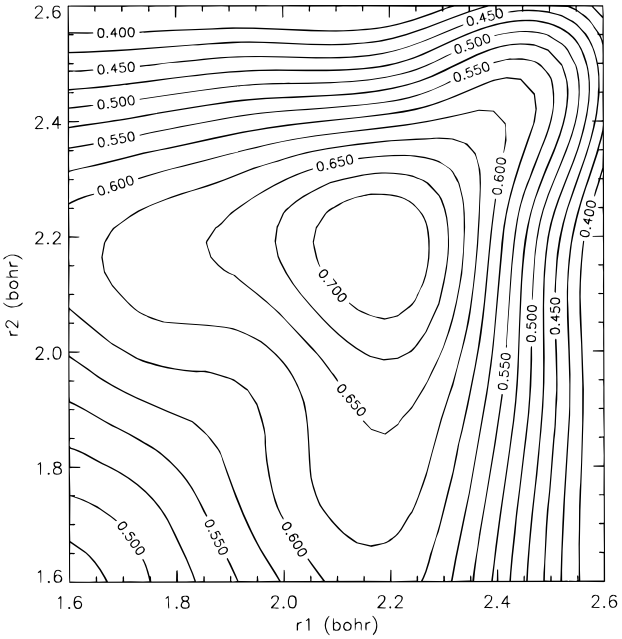

Figure 5. Two-dimensional contour plot of the *z*-component of the geometry-dependent dipole transition moment $2^2A'' \leftarrow X^2A''$ in au at the ground state eq. bond angle of 102.4° as a function of the internal coordinates (r_1, r_2). The ground state eq. geometry is at $r_1 = r_2 = 1.954$ a_0. Contour levels as indicated in Figure 3.

that through the $3^2A'$ state. In geometrical configurations in which the point group of the molecule is lowered to C_s, the *z*- and the *y*-components of the electronic transition dipole moment are both allowed to be nonzero. In accordance with the expectations, the *z*-component remains larger than the *y*-component at most geometries. A contour plot of this *z*-component of the transition moment surface is shown in Figure 5. It is seen that it decreases at most geometries inside the Franck−Condon region with respect to the constant transition dipole moment of 0.607 au at $r_1 = r_2 = 1.954$ a_0, i.e. at the ground state eq. bond lengths.

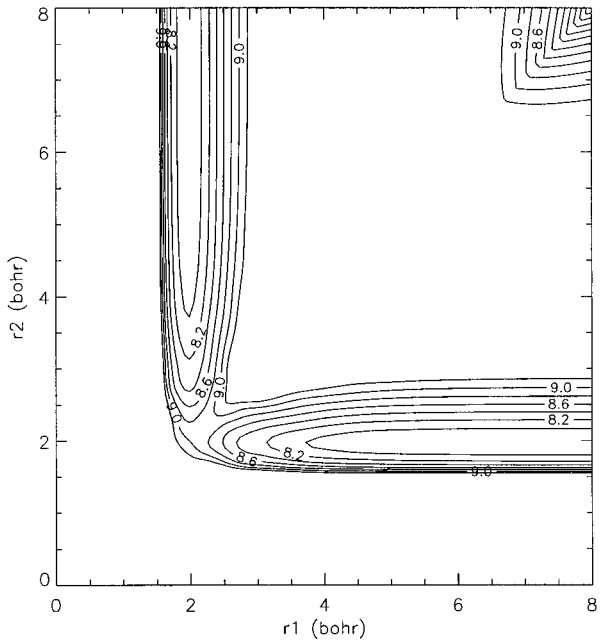

Figure 6. Two-dimensional contour plot of the potential energy surface of the $3^2A''$ state of NH_2 at the ground state eq. bond angle of 102.4° as a function of the internal coordinates (r_1, r_2). The ground state eq. geometry is at $r_1 = r_2 = 1.954$ a_0. Contour levels as indicated in Figure 2.

The PES of the $3^2A''$ state is purely repulsive along the minimum energy paths at constant r_1 (r_2) = 1.95 a_0 (Figure 6). The derivative of the potential energy at the Franck−Condon point is largest perpendicular to the $r_1 = r_2$ line, i.e. in the direction of the antisymmetric stretching coordinate. The interaction with the $4^2A''(3^2B_1)$ state leads to an avoided crossing at bond lengths slightly larger than that at the ground state eq. geometry.[6] The nodal line on the surface of the *y*-component of the transition dipole moment also reveals the avoided crossing (Figure 7). It is also seen that the *y*-component of the transition dipole moment from the ground state strongly increases up to a factor of 4.05 with respect to its value 0.112 au at the ground state eq. geometry at the large $r_{1,2}$ boundary of the Franck−Condon region. Toward N−H bond lengths smaller than that at the ground state eq. geometry, the transition dipole moment decreases. Its zero transition inside the Franck−Condon region and the increase of the transition dipole moment toward larger NH bond lengths, where the potential energy is lower, are expected to strongly influence the photodissociation dynamics through this state. Therefore a significant non-Franck−Condon contribution to the total and partial cross sections is to be expected for the $3^2A''$ state (cf. section 4.3).

For the $3^2A'$ and $2^2A''$ states the asymptotic energies are higher by several electronvolts along the $r_1 = r_2$ line. The $3^2A''$ state has a lower-lying asymptote along the $r_1 = r_2$ line, which lies nevertheless above the lowest asymptotes by 0.95 eV. Therefore dissociation into N + H + H product channels is virtually prevented compared with that into the lower-lying NH + H channels.

3. Method and Parameters of Dynamics Calculations

3.1. Method. The 2D total and partial photodissociation cross sections have been calculated by a time-dependent wave-packet propagation method along the lines of that developed by Schinke,[18] which has been developed for triatomic molecules in C_{2v} symmetry in the light−heavy−light (LHL) approximation using internal coordinates r_1 and r_2.[19] In the LHL approximation

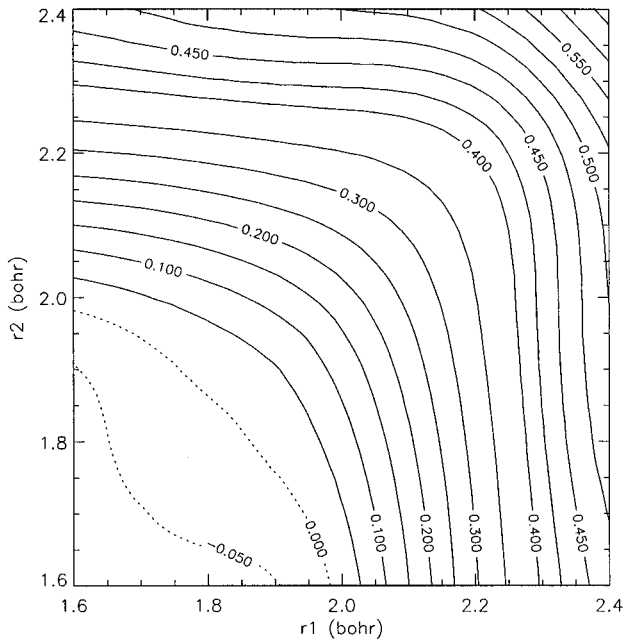

Figure 7. Two-dimensional contour plot of the *y*-component of the geometry-dependent dipole transition moment $3^2A'' \leftarrow X^2A''$ in au at the ground state eq. bond angle of 102.4° as a function of the internal coordinates (r_1, r_2). The ground state eq. geometry is at $r_1 = r_2 = 1.954$ a_0. The numbers at the contour levels denote the electric dipole transition moment in au. Contour levels as indicated in Figure 3.

all terms of the Hamiltonian proportional to the inverse of the mass of the heavy central atom are neglected.

The cross section can be calculated either as the Fourier transform of the autocorrelation function $S(t)$[20]

$$\sigma(\omega) = \frac{\omega}{6\epsilon c}\int_{-\infty}^{\infty}\exp(i(E_0 + \hbar\omega)t/\hbar)\cdot S(t)\,dt \qquad (1)$$

with

$$S(t) \equiv \langle\Phi(r_1, r_2, t{=}0)|\Phi(r_1, r_2, t)\rangle \qquad (2)$$

$\Phi(r_1,r_2,t{=}0)$ equal to the product of the electric transition dipole moment $\mu(r_1,r_2)$, and the normalized vibrational ground state wave function $\Theta^0(r_1,r_2)$. The dependence of the electronic part of the electric transition dipole moment on the internal coordinates r_1, r_2 of the nuclei is taken into account within the Born Oppenheimer approximation. This way part of the non-Franck−Condon contributions to the total cross section are taken into account. The total cross section can alternatively be represented as the sum of the partial cross sections with respect to the vibrational fragment states:

$$\sigma(\omega) = \sum_v \sigma_v(\omega) \qquad (3)$$

The partial cross sections result from the projection of the wave packet $\Phi(r_1,r_2,t)$ on a particular fragment channel $\Phi_v(r_1)$ in the asymptotic range of the potential energy surface

$$\sigma_v(\omega) = \frac{4\pi^2\omega k_v}{3\hbar c\epsilon_0\mu_d}\cdot|A_v(r_{2,\infty},\omega)|^2 \qquad (4)$$

with k_v given by

$$k_v = \frac{1}{\hbar}\sqrt{2\mu_d(\hbar\omega + E_0 - e_v)} \qquad (5)$$

with μ_d denoting the reduced mass of the diatomic fragment, ϵ_v being the energy of the diatomic fragment in its v-state, and E_0 being the energy of the initial state, i.e. the vibrational ground state, from which the excitation starts. $A_v(r_{2,\infty},\omega)$ is equal to

$$A_v(r_{2,\infty},\omega) = \frac{1}{2\pi}\int_{t=0}^{\infty}\exp(i(\hbar\omega + E_0)t/)\,\langle\Phi_v(r_1)|\Phi(r_{2,\infty}, r, t)\rangle \qquad (6)$$

The factor 2, which occurs in eq 4 in addition to the prefactor of the partial cross sections of a linear triatomic in Jacobi coordinates (cf. eq 7 of ref 21, eq 6 of ref 22, in which the reduced mass of the molecule μ_c replaces that of the diatomic fragment μ_d), arises from the existence of two different, however indistinguishable, fragmentation channels for symmetric triatomic molecules.

The time-independent vibrational eigenfunctions of the ground state are obtained from a variational procedure. As a basis set, 12−18 Morse oscillator functions are employed along each coordinate. The integrals involving the ground state potential are calculated by the Gauss−Laguerre quadrature. The wave function at time t, $\Phi(r_1,r_2,t)$, is obtained by application of the time evolution operator on $\Phi(r_1,r_2,0)$

$$\Phi(r_1, r_2, t) = e^{-(i/\hbar)Ht}\cdot\Phi(r_1, r_2, 0) \qquad (7)$$

H denotes the Hamiltonian for nuclear motion in the LHL approximation

$$H = -\frac{\hbar^2}{2\mu_c}\frac{\partial^2}{\partial r_2^{\,2}} - \frac{\hbar^2}{2\mu_d}\frac{\partial^2}{\partial r_1^{\,2}} + V(r_1, r_2) \qquad (8)$$

with μ_c and μ_d denoting the reduced masses of the two indistinguishable NH fragments

$$\mu_{c,d} = \frac{m_N\cdot m_{H_{1,2}}}{m_N + m_{H_{1,2}}} \qquad (9)$$

The Hamiltonian of eq 8 is isomorphous to the Hamiltonian for nuclear motion in linear triatomic molecules in Jacobi coordinates (e.g. ref 23) with r_1 formally replaced by r, r_2 replaced by R, and the reduced masses $\mu_{c,d}$ of the two identical NH fragments replaced by the reduced mass of the complex (μ_c) and of the diatomic fragment (μ_d), respectively. The LHL approximation implies that the coupling terms of the kinetic energy operator involving the two stretching modes and the corresponding stretching−bending coupling terms are neglected. Since the main deviations of the full 3D result from the 2D LHL and 3D LHL results arise from H_{s-s}, the 2D LHL and 3D LHL results for the vibrational fragment distributions are in very good agreement. H_{s-s} vanishes for a bond angle of 90°. Therefore the LHL approximation is most suitable for molecules with an equilibrium bond angle around 90°. Mainly for this reason the LHL approximation is better applicable to H_2O with a ground state equilibrium bond angle around 104° than to CH_2 with a ground state equilibrium bond angle around 134°.[24]

Since NH_2 has a mass ratio m_H/m_X (m_X: mass of the heavy atom) between the mass ratios for CH_2 and H_2O, and since at the same time the equilibrium bond angle of NH_2 is still closer to 90° compared with H_2O (102.4° vs ∼ 104°), it can be assumed that the LHL approximation is fully applicable to NH_2 also. Calculations including the coupling term in the kinetic energy operator are within the present computational scope and have also been performed e.g. for the first excited state of H_2O.[25] Although the contribution of the coupling term to the total cross section and to the individual partial cross sections is estimated to be small here, inclusion of the coupling term turns out to be

important in other cases, namely in order to obtain correct intensity ratios in emission to pairs of vibrational states with different symmetric and antisymmetric (υ_s, υ_a) quantum numbers.[25]

The character of the periodic or vibrational motion which can be assigned to the maxima of the total cross section of photodissociation or photoabsorption can be inferred from a contour plot of the stationary wave function $\Phi(r_1,r_2,E_0)$ at the resonance or bound state energy E_0 which is given by the Fourier transform of the wave packet:

$$\int_{-\infty}^{+\infty} \Phi(r_1, r_2, t)\cdot\exp\{iE_0t/\hbar\}\, dt \qquad (10)$$

For a potential with the shape of a rotational paraboloid with its main axes of inertia along $\vec{r}_1$ and $\vec{r}_2$, the nodal planes of the two stretching normal modes would be parallel and perpendicular, respectively, to r_1 and r_2. If two minima occur on the potential energy surface of a symmetric triatomic, which are separated by a small barrier allowing interaction between the two potential troughs, the vibrational levels υ_1 and υ_2 in each of the two potential troughs are split by the interaction. The resulting wave functions of the interacting vibrational levels are either symmetric or antisymmetric with respect to the $r_1 = r_2$ line. For symmetry reasons, from the $\upsilon = 0$ ground state vibrational level only transitions into symmetrically coupled levels are allowed, i.e. levels with a wave function symmetric to the $r_1 = r_2$ line. If the potential is strongly anharmonic, additional coupling may arise between the symmetrically coupled levels of the antisymmetric and symmetric stretching normal modes. Examples for the analysis of the nodal structure of stationary wave functions of bound vibrational levels and at the energies of vibrational resonances will be given in section section 4.

In the application of the kinetic energy operator on the excited state wave function the Fast Fourier Transform algorithm[26] has been used. The time propagation of the wave packet has been performed by applying the short iterative Lanczos integrator.[27]

In order to prevent reflections of the wave packet from the asymptotic range into the Franck−Condon region of the excited state PESs, which could falsify the Fourier transform of the autocorrelation function, the wave function is multiplied with an absorption function defined by

$$f_{cut} = 1 \quad (\text{for } \gamma < 0)$$
$$f_{cut} = 6\gamma^2(1-\gamma) \quad (\text{for } \gamma < 0.5)$$
$$f_{cut} = 1 - 2(1-\gamma)^3 \quad (\text{for } \gamma > 0.5)$$
$$f_{cut} = 0 \quad (\text{for } \gamma > 1) \qquad (11)$$

with $\gamma = (r_{max} - r)/(r_{max} - r_{min})$, with r_{min} and r_{max} being the minimum and maximum values of the range of r_1, r_2 in which a nonconstant absorption function is applied.

Subsequent spline fits in both dimensions of the 2D surface have been used in order to represent the electronic potential on a dense and regular grid as a function of the bond coordinates.

3.2. Parameters of Dynamics Calculations. The extension of the initial wave function, given by the width at which it has decreased to 1/e of its maximum absolute value, is 0.56 a_0 along both r_1 and r_2.

A vertical excitation energy of 7.53 eV has been calculated for the electronic transition from the ground state to the $3^2A'$ state, i.e. without taking into account the zero-point energy.[6] Since the energies of the two indistinguishable $NH(A^3\Pi) + H$ asymptotes are 7.78 eV,[6] it follows that the fragmentation through this state will be extremely slow and that the major contribution to the total and partial cross sections will arise from resonant levels or from the dissociation continuum with excitation energies close to the dissociation limit. Test calculations, in which different point densities have been employed for the grids of the PES in a N−H bond distance range from 1.3 to 10.0 a_0, have shown that the major contribution to the total and partial cross sections arises from the excitation energy range of 0.6 eV above the dissociation limit. Thus the wave packet will take up at the most about 0.6 eV of kinetic energy. With the reduced mass of 0.94·1822.89 au for the dissociating hydrogen atom, a maximum wavenumber k of 8.7 au results. This leads to a minimum grid spacing of 0.361 a_0 meaning that in a range from 1.3 to 10.0 a_0 more than 22 grid points are required along each of the two bond coordinates r_1 and r_2. In order to allow the NH fragment to take up the same amount of kinetic energy, a point density larger by a factor of $(m_{NH}/m_H)^{1/2} \sim 3.7$ is needed. The resulting minimum number of points per dimension is 82. In order to achieve a smooth representation of the PES, the point density was increased to 140 × 140 points. In order to allow the initial wave function to escape from the grid with a probability of 23%, a propagation time T of 4800 fs is needed. The minimum energy $\Delta E = \pi/T$ which can still be resolved with this choice of the propagation time is 0.0004 eV. This turns out to be sufficient for the resolution of the sharpest resonance line with a full width at half-maximum (fwhm) of 0.0012 eV. In order to cover an excitation energy range up to 8.5 eV, a time step of less than 10.0 au has to be chosen for the propagation.

The $2^2A''$ state has a vertical electronic excitation energy of 7.60 eV.[6] The energy of the lowest (indistinguishable) $NH(a^1\Delta) + H$ asymptotes is 5.75 eV. Thus the dissociating hydrogen atom can be provided with a kinetic energy of at most about 1.8 eV. Inside the width of the initial wave packet the potential energy increases by about 0.5 eV. In total a kinetic energy range of 2.3 eV for the dissociating atom should be described. This corresponds to a grid spacing of 0.26 a_0 per dimension. If the NH fragment is allowed to take up the same kinetic energy, a point density of 90 points is needed for each dimension in a coordinate range from 1.2 to 8 a_0. In practice, grids of 96−120 points per dimension have been used. The resolution of the vibrational substructure of the cross sections requires an energy resolution which is smaller by at least 1 order of magnitude compared with the vibrational frequencies of NH_2 in this state. Propagation times between 60 000 and 200 000 au corresponding to energy resolutions between 0.0014 and 0.0004 eV have been used. The time step has been set to 6 au.

The $3^2A''$ state with a vertical excitation energy of 9.07 eV[6] shares its lowest asymptotes with the $3^2A'$ state. The minimum energy paths run parallel to the r_1 and r_2 axes, with the second N−H bond length equal to 1.95 a_0. Local minima do not occur along these paths. The kinetic energy released to the dissociating fragments is 1.26 eV. This is expected to be distributed between the H and the NH fragments according to their inverse mass ratio. If, however, the heavier NH fragment is allowed to take up the same amount of kinetic energy as the hydrogen atom, a grid spacing of 0.06 a_0 and a point number of 109 along each bond coordinate in a range from 1.2 to 8 a_0 are required. A propagation time of 60 000 au was also used here, corresponding to an energy resolution of 0.0014 eV. A time step of 4 au has been used.

4. Results and Discussion

For the zero-point energy of the $X^2\ A''$ state an energy of 0.432 eV has been calculated using a variational procedure on

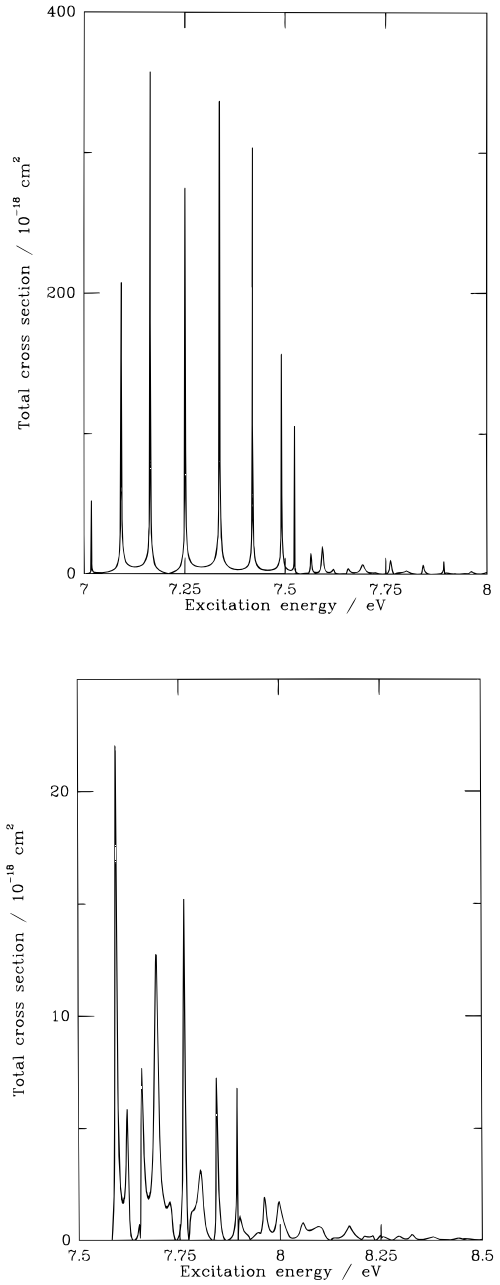

Figure 8. Total cross section of photodissociation through the $3^2A'$ state as a function of excitation energy: (a) lower excitation energy range with bound and resonant vibrational levels and (b) higher excitation energy range above bound range of the potential, resonant vibrational levels. The *y*-scale is different in (a) and (b).

the space of Morse oscillator basis functions. This is in good accordance with the experimental result of 0.404 eV resulting from the symmetric and antisymmetric stretching frequencies measured by high-resolution Fourier transform IR spectroscopy.[28] The following results for the total cross sections from the Fourier transform of the ACF and from the sum of the partial cross sections are in accordance to better than 0.02×10^{-18} cm^{-2}.

4.1. Photodissociation through the $3^2A'(2^2A_1)$ State. In accordance with the bound state character of the $3^2A'$ state photodissociation through this state is a slow fragmentation process, which is, however, interesting due to the multiline vibrational structure of the total cross section, arising from bound and long-lived resonant vibrational levels (Figure 8a). In accordance with the existence of bound vibrational levels about 77% of the wave packet remains in the bound region of the PES. The nodal line of the transition dipole moment between $r_1 = 2.75-3\ a_0$ at variable r_2 lies outside the Franck−Condon region and does not therefore affect the results of the dynamics calculations significantly.

TABLE 1: Maxima in the Fourier Transform of the Autocorrelation Function Assigned to Most Pronounced Bound and Resonant Stretching Vibrational Levels in the $3^2A'$ State of NH_2; Assignment Given in Text. Weaker Splitting Components by Fermi Type Interactions Are Not Counted as Separate Lines

line no.	excitation energy	line no.	excitation energy
1	7.0195	14	7.7266
2	7.0931	15	7.7689
3	7.1652	16	7.7887
	7.2461	17	7.8135
4	7.2580	18	7.8454
5	7.3383	19	7.8957
6	7.4208		7.9129
	7.4458		7.9390
7	7.4930	20	7.9484
8	7.5250	21	7.9719
9	7.5638	22	7.9964
10	7.5819	23	8.0136
11	7.6014	24	8.0345
	7.6463	25	8.0674
12	7.6557	26	8.0945
	7.6729	27	8.1519
13	7.7000	28	8.1816

As expected the vibrational substructure of the total cross section clearly differs from that found in the 1D treatment by Saxon et al.,[14] in which only two maxima had been found in the total cross section (cf. section 1). The nine lines which are lowest in excitation energy correspond to bound vibrational levels. For these levels, which are infinitely sharp in energy within the nonrelativistic quantum mechanical description, the line widths are artificially induced by the finite propagation time in the calculation.

The vibrational motion at the energies of the bound levels and the resonances can be analyzed by inspection of the nodal structure of the stationary wave function given by the Fourier transform of the wave packet (cf. section 3). In what follows the notation for the antisymmetric and symmetric stretching levels v_1 and v_2 in one individual potential trough isolated from the other one is used. Due to the particular shape of the PES of this state (Figure 2), the symmetric stretching mode can be characterized as one with nodal planes parallel to the dissociation coordinates $r_{1,2}$ at large bond distances and perpendicular to the $r_1 = r_2$ line in the coordinate range of the saddle point, whereas the antisymmetric stretching mode has wave functions with nodal planes perpendicular to the dissociation coordinates $r_{1,2}$ at large bond distances and parallel to the $r_1 = r_2$ line in the coordinate range of the saddle point.

The excitation energies at which the bound vibrational levels and resonances occur are listed in Table 1. The bound state line at the lowest excitation energy in Figure 8a corresponds to the totally symmetric vibrational level without any nodal planes and with its maxima at the two identical minima of the PES (Figure 9a). The zero-point energy including symmetric and antisymmetric stretching motion on this PES amounts to 0.236 eV. The lowest vibrational level lies already above the small barrier between the potential troughs by 0.084 eV. The stationary wave function of the second bound vibrational state has one nodal plane at each of the two local minima of the PES, perpendicular to the $\vec{r}_1$ and $\vec{r}_2$ axes, respectively. In accordance with the derivatives along $\vec{r}_1$ and $\vec{r}_2$ at the two minima, this line is assigned to the symmetrically coupled $v_2 = 1$ levels of the antisymmetric stretching motion in each of the two identical troughs (Figure 9b). An energy quantum of

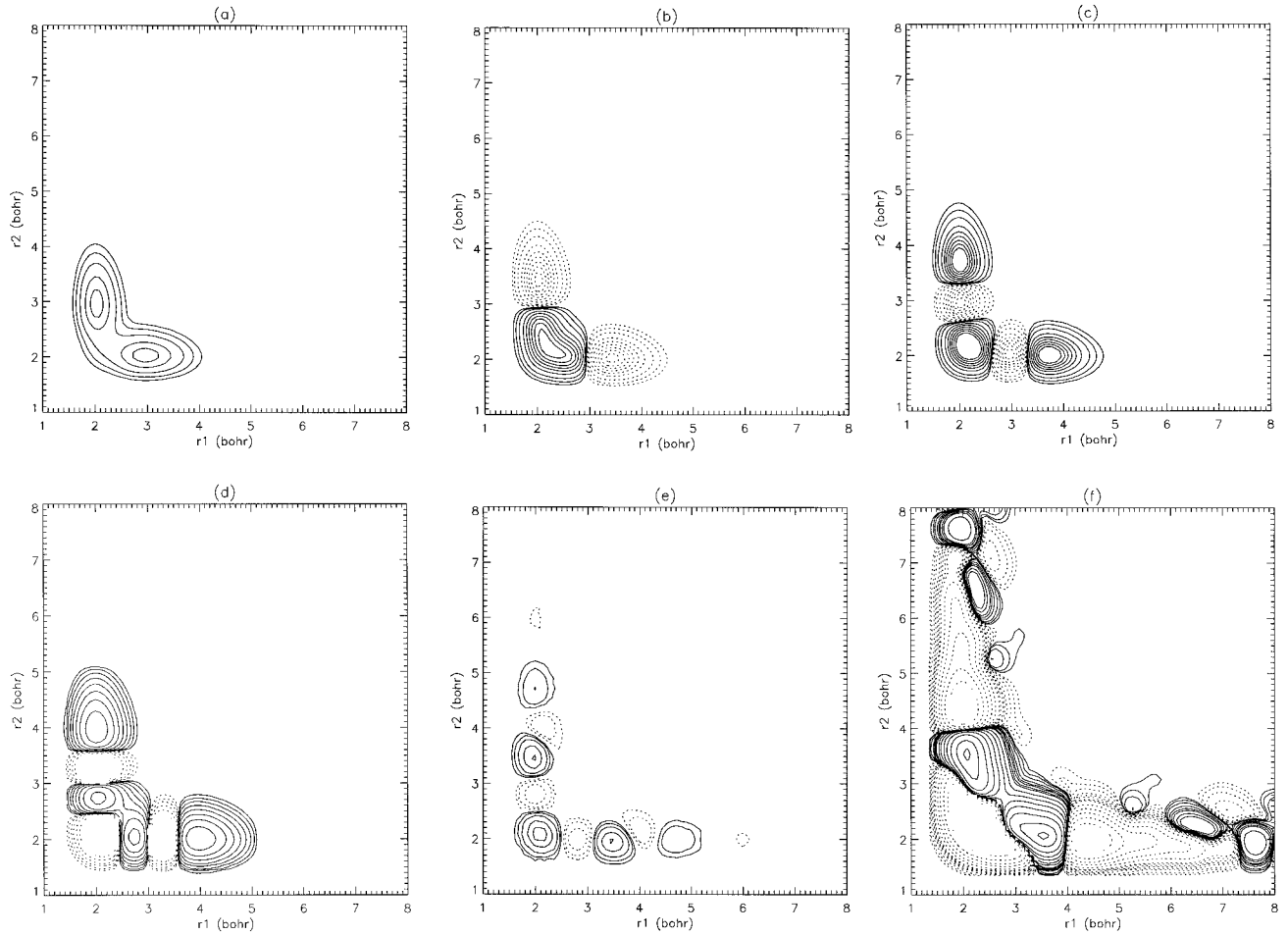

Figure 9. Contour plots of stationary wave functions at various bound state and resonance energies, respectively, corresponding to the excitation energies of (a) 7.0195, (b) 7.0931, (c) 7.1652, (d) 7.2524, (e) 7.8957, and (f) 8.0945 eV.

0.074 eV results for the antisymmetric stretching motion. This also agrees with the longer recurrence periods of about 56 fs in the ACF. From the zero-point energy of 0.236 eV and the energy quantum of 0.074 eV for the antisymmetric stretching motion, a symmetric stretching quantum of 0.398 eV follows for the lowest symmetric stretching level. The strong anharmonicity of the potential may however cause deviations from the harmonic oscillator behavior already in the low-lying stretching levels; i.e. the lowest symmetric stretching level presumably occurs at lower energy than 0.398 eV above the totally symmetric level. The third line in the Fourier transform of the ACF is assigned to the symmetric combination of the $v_2 = 2$ levels in each of the two potential troughs (Figure 9c). The stationary wave function has two nodal planes mainly perpendicular to $\vec{r}_1$ and $\vec{r}_2$, respectively. Again only the symmetric combination of these levels is seen in the spectrum. The reduced energy difference of 0.072 eV between the third and second level may result from a weak interaction with the $v_1 = 1$ level. Since the energy quanta of the antisymmetric stretching motion are small compared with those of the symmetric stretching motion, several levels of the antisymmetric stretching motion are involved in the interactions with the v_1 levels. The $v_1 = 1$ level is split by a Fermi resonance with the symmetric combination of the $v_2 = 3$ levels into two components with an energy separation of 0.004 eV. The nodal structure in both components shows the interaction (cf. Figure 9d, for one component). The shift of the fourth bound state line toward higher excitation energy is caused by this interaction. Weaker interactions of $v_1 = 1$ involve the $v_2 = 2$ and the $v_2 = 4$ and 5 levels. The splittings of these v_2 levels in the low-energy range (bound spectrum) are smaller than the minimum resolvable energy difference of 0.0004 eV and are therefore not seen in the spectrum. The fifth bound level at an excitation energy of 7.338 eV corresponds to the symmetric combination of the $v_2 = 4$ levels perturbed by $v_1 = 1$. Due to the smaller amplitudes of the wave functions at higher v_2 and v_1 quantum numbers, the nodal structure of the higher lying levels can only be resolved close to the spatial maxima of the wave functions. Therefore the nodal structure of the wave functions corresponding to higher lying bound levels is only clear in the coordinate range close to the maximum of the absolute value of the wave function. Furthermore the infinitely small line widths of the bound and the small line widths of the order of 0.001 eV of some resonant levels render it very difficult to hit the energies of these levels within their fwhm induced either by the finite propagation time or their natural life time. An unambiguous assignment is therefore not possible for the higher-lying sharp levels. Besides the nodal structure, the tentative assignment of the higher-lying bound levels and the resonances given in this work is based on an extrapolation of the sequence of the lower-lying vibrational levels. The sixth level at 7.421 eV presumably corresponds to $v_2 = 5$ interacting with $v_1 = 1$. Approaching the dissociation limit, the strong anharmonicity of the potential increases the density of antisymmetric and symmetric stretching levels. In this excitation energy range, on average one symmetric stretching level interacts with the two adjacent antisymmetric levels. This leads to the 3-fold split features close to the dissociation limit. The levels at 7.446, 7.493, and 7.524 eV presumably correspond to the interaction of the (symmetrical combinations of) the levels $v_1 = 2$, $v_2 = 6$, and $v_2 = 7$. The one at 7.446 eV

has a very small overlap with the $v = 0$ ground state vibrational level and does therefore not contribute to the Fourier transform of the ACF. The level at 7.564 eV is expected to arise from the interaction of the $v_1 = 3$ and the $v_2 = 8$ and 9 levels. This feature smoothly extends into the photodissociation continuum.

The ground state $v = 0$ vibrational level has its largest overlap with the low-lying bound symmetrically coupled antisymmetric stretching vibrational levels of the $3^2A'$ state. Its overlap with the rapidly oscillating wave functions of the dissociation continuum is small. This means that photodissociation through this state will mainly proceed through resonant stretching motion. In accordance with the increasing interaction with the photodissociation continuum toward higher excitation energy, the resonance lines are gradually more broadened above the dissociation limit. Yet resonance lines with line widths as small as 0.001 eV are found, e.g. for the sharp resonance line at 7.896 eV.

The first two resonance lines at excitation energies of 7.582 and 7.601 eV are expected to correspond to the higher-lying splitting components from the $v_1 = 3$ and $v_2 = 8$ and 9 interaction. The next three resonance lines at 7.656, 7.673, and 7.700 eV arise from the interaction of the $v_1 = 4$ and $v_2 = 10$ and 11 levels. The small additional splitting of the first of the three levels may result from the interaction with the adjacent $v_1 = 3$ levels. Due to the large anharmonicity of the potential, the wave functions of the three levels interchange their character. Therefore all three components contribute to the photodissociation spectrum. The coupling of symmetric and antisymmetric stretching motion is particularly important in this case of slow photodissociation in order to direct part of the flux into the dissociation channels. Above 7.75 eV the splitting pattern becomes irregular due to the increasing overlap with the direct photodissociation continuum. The most long-lived sharp resonances at 7.769, 7.845, and 7.896 eV with line widths between 0.001 and 0.002 eV, corresponding to life times between 326 and 653 fs, mainly arise from antisymmetric stretching motion (Figure 9e). The broader and smaller resonances all correspond to combined symmetric−antisymmetric stretching motion. This is obvious from the stationary wave functions at the resonances, e.g. at 8.095 eV (Figure 9f).

Since the equilibrium bond angle in the $3^2A'$ state is similar to that in the ground state, it is expected that the vibrational substructure of the total cross section remains mainly unchanged in a 3D treatment. However, a broadening of the resonances might arise from the interaction with the bending motion.

The total cross section of photodissociation through this state integrated over excitation energy yields 0.937×10^{-18} cm^{-2}·eV. Eighty-eight percent of the NH fragments are found in the $v' = 0$ vibrational level of the $^3\Pi$ state. The shape and substructure of the $v' = 0$ partial cross section (Figure 10) and the total cross section (Figure 8a,b) are very similar. Vibrationally excited fragments are only produced at excitation energies higher than 7.94 eV ($v' = 1$) and 8.28 eV ($v' = 2$) (Figure 10). The integrated $v' = 1$ partial cross section yields 10% of the total integrated cross section, whereas the contribution of the integrated $v' = 2$ partial cross section is 1.3%. At excitation energies higher than 7.9 eV the $v' = 1$ vibrational fragment state is preferred. Its partial cross section provides the dominant contribution to the total cross section, i.e. 57% compared with 34% from the $v' = 0$ partial cross section, both with respect to the integrated total cross section in this excitation energy range. From the analysis of the stationary wave functions at the resonance energies, it is seen that the symmetric stretching motion is highly excited in this excitation energy range. Only here the excitation energy is sufficient for leaving the NH fragment in the $v' = 1$ level of the $A^3\Pi$ state. The $v' = 3$ partial cross section integrated over the full excitation energy range contributes by less than 0.2%.

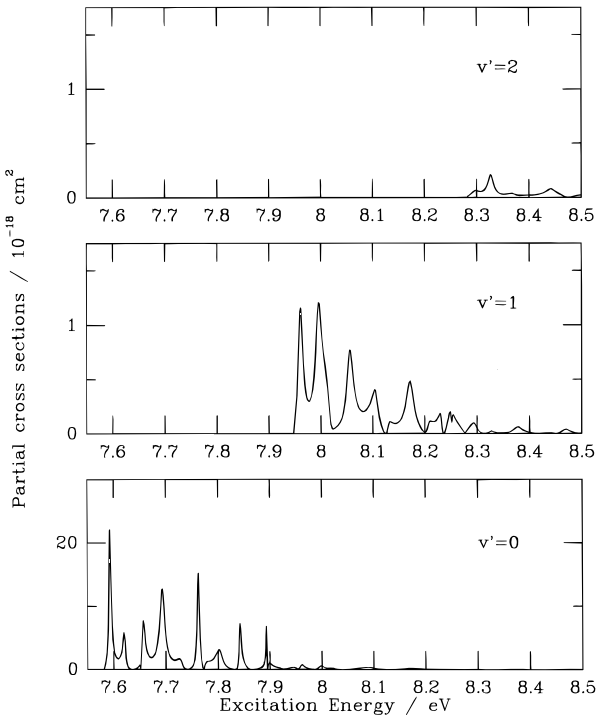

Figure 10. Partial cross sections of photodissociation through the $3^2A'$ state as functions of excitation energy. v' denotes the vibrational quantum number in the NH($A^3\Pi$) fragment state.

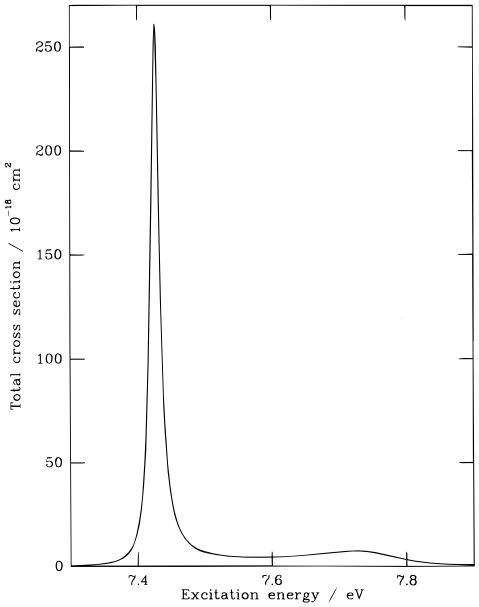

Figure 11. Total cross section of photodissociation through the $2^2A''$ state as a function of excitation energy.

4.2. Photodissociation through the $2^2A''(2^2B_1)$ State. The total cross section of photodissociation through the 2^2 A″ state is shown in Figure 11. This cross section includes the contributions from both components of the electric transition dipole moment in the A′ representation of the C_s point group. As expected, the surface of the *z*-component of the transition dipole moment yields almost the total intensity of the spectrum. The contribution of the *y*-component to the total cross section, which vanishes at the ground state equilibrium geometry for symmetry reasons, amounts to only 3% of the total integrated cross section. In contrast to the $3^2A'$ state, the 2^2 A″ total cross

section shows only a single pronounced resonance at an excitation energy of 7.426 eV. This excitation energy is higher by 0.11 eV than the barrier to dissociation. The line width of the resonance is 0.015 eV (fwhm), corresponding to a life time of 43.5 fs for the resonant level. The nodes of the stationary wave function at the resonance energy are perpendicular to the dissociation coordinates parallel to the r_1 and r_2 axes. Apart from a strong maximum in the region of the local minimum of the PES, the probability amplitude of the wave function along the $r_1 = r_2$ line is zero. This nodal structure shows that the resonant photodissociation process proceeds via antisymmetric stretching motion. The broad, shallow maximum at 7.72 eV excitation energy corresponds to direct photodissociation. Its maximum intensity is 7.351×10^{-18} cm^{-2}. From comparison of the absolute values of the total cross section it is already obvious that photodissociation through this state is much more efficient than through the $3^2A'$ state. The total cross section integrated over excitation energy yields 8.332×10^{-18} cm^{-2}·eV, of which 97% arises from the dominant *z*-component of the transition dipole moment. This integrated total cross section is about 88% of the result obtained from a calculation based on the constant transition dipole moment, since the dominant *z*-component of the transition dipole moment decreases at most geometries inside the Franck−Condon region with respect to the constant transition dipole moment of 0.607. The *y*-component of the transition dipole moment, through which the transition from the ground state is symmetry-forbidden at the ground state eq. geometry, yields only 3% of the total integrated cross section and does not alter the shape of the total cross section significantly. More than 96% of the NH fragments from dissociation through this state are produced in the vibrational fragment level $v' = 0$ of the NH $^2\Delta$ state. The structure of the $v' = 0$ partial cross section corresponds very well to that of the total cross section. The partial cross section $v' = 1$ only contributes by 3.5%, whereas the contributions of the vibrational fragment states $v' = 3$ and 4 are 0.2% and 0.01% only. All partial cross sections have essentially the same structure as the total cross section (Figure 11) and are therefore not shown separately.

4.3. Photodissociation through the $3^2A''(1^2A_2)$ State. The total cross section through the 3^2 A″ state is shown in Figure 12a. Figure 12b displays the non-Franck−Condon contribution of the *z*-component to the total cross section which vanishes at the ground state eq. geometry for symmetry reasons (note that the *y*-scales are different in parts a and b of Figure 12. The shape of the total cross section is determined by the purely repulsive nature of this state and by the avoided crossing with the $4^2A''(3^2B_1)$ state.[6] The latter leads to a zero transition in the *y*-component of the transition dipole moment close to the ground state eq. geometry (Figure 7). The intermediate minimum of the total cross section in Figure 12a at 9.24 eV arises from this nodal line. For comparison the result for the total cross section through this state has also been computed by means of the constant transition dipole moment of 0.112 au at the ground state eq. geometry. From this calculation it was seen that the intermediate minimum does not occur here and that the maximum of the total cross section is smaller by a factor of about 5. This is feasible since Figure 7 shows that the dominant component of the transition dipole moment rapidly increases toward larger N−H bond lengths, up to a factor of about 4 at the outer boundary of the Franck−Condon region, and that the maximum of the total cross section is found for the broad continuum feature at lower excitation energy. The most pronounced feature of the total cross section with a maximum at 8.75 eV and with a width of 0.50 eV contains

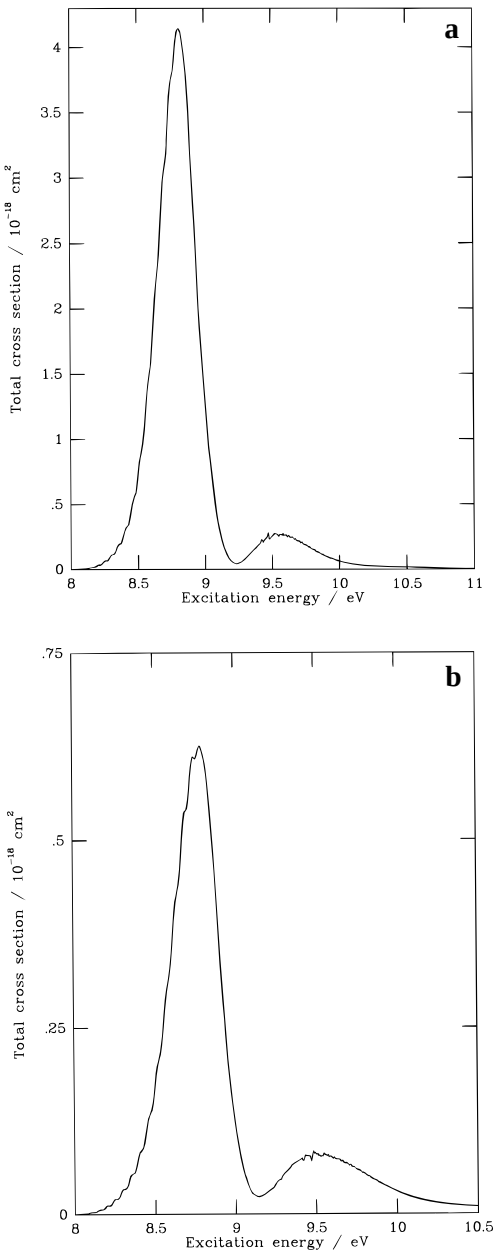

Figure 12. (a) Total cross section of photodissociation through the $3^2A''$ state as a function of excitation energy. (b) Non-Franck−Condon contribution to the total cross section of (a), arising from the *z*-component of the geometry-dependent dipole transition moment (Figure 7b). The *y*-scale is different in (a) and (b).

93% of the total cross section of photodissociation through this state integrated over excitation energy. The smaller continuum feature at higher excitation energy has its maximum at 9.53 eV. Both features of the total cross section are mainly caused by direct photodissociation and thus reflect the purely repulsive potential of this state. The diffuse substructure in the low-excitation energy slope of the most pronounced feature in Figure 12a,b is due to short-lived vibrational resonances from coupled antisymmetric−symmetric stretching motion. In accordance with the gradient of the PES being lowest along the symmetric stretching coordinate $r_1 = r_2$, symmetric stretching motion is primarily excited at the resonance energies. The anharmonicity of the potential induces strong coupling between adjacent resonant symmetric and antisymmetric stretching levels. This coupled motion transfers part of the flux from the Franck−Condon region of the PES into the dissociation channels. The natural line widths of these weak resonances are larger than

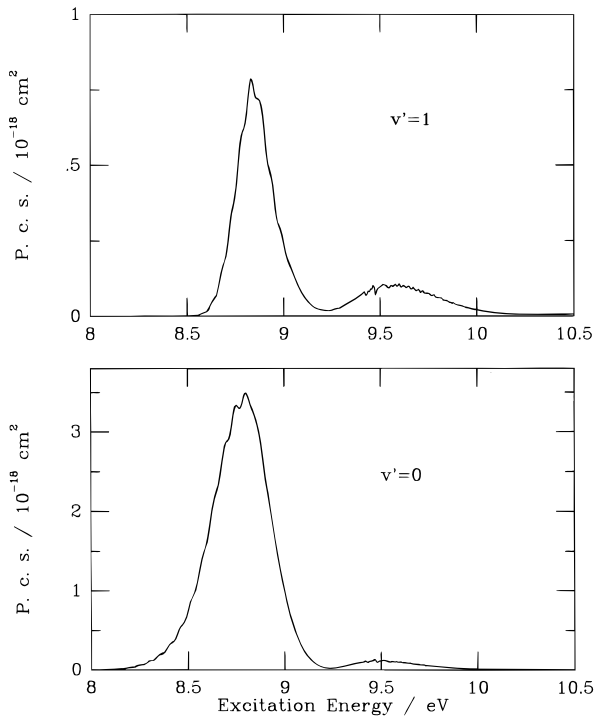

Figure 13. Partial cross sections of photodissociation through the $3^2A''$ state as functions of excitation energy. v' denotes the vibrational quantum number in the NH($A^3\Pi$) fragment state.

0.019 eV corresponding to life times shorter than 35 fs. Toward higher excitation energies the life times of the resonances decrease. The energy quanta of about 0.05 eV of this mode corresponds to recurrence periods of about 82 fs in the ACF.

The partial cross sections of photodissociation resolved with respect to the vibrational fragment quantum numbers $v' = 0$ and $v' = 1$ are shown in Figure 13. The contributions of higher-lying vibrational fragment levels are smaller than 5% of the $v' = 0$ partial cross section of Figure 13. The latter essentially corresponds to that of the total cross section in its shape and vibrational substructure and yields 82% of the total cross section integrated over excitation energy. For the $v' = 1$ fragment state, the integrated partial cross section of Figure 13 amounts to 15% of the integrated total cross section.

The integrated cross section of photodissociation through this state amounts to 1.640×10^{-18} cm^{-2}·eV. With the relatively small constant transition dipole moment of 0.112 au at the ground state eq. geometry, an integrated cross section of only 0.316×10^{-18} cm^{-2}·eV results. This comparison shows that it is absolutely essential to take the geometry dependence of the transition dipole moment into account in this case. The most dominant contribution to the integrated total cross section, i.e. 82%, arises from the *y*-component of the electric transition dipole moment. However, a significant non-Franck−Condon contribution to the total cross section stems from the *z*-component of the electric transition dipole moment which vanishes at the ground state eq. geometry.

In a full 3D treatment including the bending motion, the diffuse resonances and the intermediate minimum from the nodal line of the transition dipole moments may be broadened and shifted in energy by the interaction with the bending motion. Small shifts in energy may also occur for the maxima of the total and partial cross sections.

4.4. Comparison with Experiment. The fluorescence intensity in the energy range 7.5−8.3 eV ("region I" in ref 15) of the experimental spectrum by ref 15 only arises from photodissociation through the $3^2A'$ state. The $2^2A''$ state lies in the same energy range but has a NH($a^1\Delta$) + H asymptote and does thus not contribute to the NH($A^3\Pi$) + H fragment fluorescence spectrum. The low-angle $2^2A'$ state dissociates into NH($b^1\Sigma^+$) + H and does therefore not contribute to this fluorescence spectrum either. The energy resolution in the experimental spectrum is given by 3 nm,[15] which corresponds to 0.28 eV around 148 nm and to 0.14 eV around 165 nm, the boundary of region I. Since the calculated energy spacing between the adjacent bound state and resonance lines is less than 0.1 eV, the calculated vibrational substructure of the $3^2A'$ cross section is not resolved in the experimental spectrum.

Photodissociation in the excitation energy range of 8.5−10 eV corresponding to "region II" of the experimental spectrum[15] is expected to proceed via the $3^2A''$ and $4^2A''$ states. The contributions of the $2^2A''$ and $3^2A'$ states to the sum of the total cross sections of the three considered states have decreased to 1% and 0.5%, respectively, of the sum of the integrated total cross sections through the $3^2A'$, $2^2A''$, and $3^2A''$ state in this energy range. Since the $4^2A''$ state does not correlate with the NH($A^3\Pi$) fragment state, only the avoided crossing of the $3^2A''$ and $4^2A''$ states close to the Franck−Condon region could lead to a significant contribution of the $4^2A''$ state to the NH($A^3\Pi$) fluorescence intensity via a nonadiabatic transition. However, since the energy and intensity of a nonadiabatic transition depends sensitively on the exact shape of the PES, the investigation of this nonadiabatic transition and photodissociation through the 3^2B_1 state must be left to a 3D treatment of photodissociation. Considering the ratio of the integrated total cross sections through the $3^2A'$ and the $3^2A''$ states, namely 0.57, a first comparison with Figure 1 from ref 15 suggests that the fluorescence intensity of region II mainly arises from photodissociation through the $3^2A''$ state and that a possible contribution of photodissociation through the $4^2A''$ state by a nonadiabatic dipole transition is weak. The experimentally detected vibrational substructure with a spacing of 0.105 eV[15] is not found in the 2D treatment of photodissociation through this state. Hence it can be expected that the vibrational substructure of region II corresponds to (coupling to) the bending mode, which will be further investigated in a 3D treatment.

5. Conclusions

Among the $3^2A'(2^2A_1)$, the $2^2A''(2^2B_1)$, and the $3^2A''(1^2A_2)$ states of NH_2, the $2^2A''$ state has by far the largest cross section of photodissociation. The integrated total cross section of photodissociation through this state amounts to 8.332×10^{-18} cm^{-2}·eV. The total cross section of photodissociation through the $3^2A'$ state is relatively small, in accordance with its bound state character. Its integration over excitation energy yields 0.937×10^{-18} cm^{-2}·eV. Since the equilibrium angle of this state differs by only 2.6° from the ground state equilibrium bond angle, the results for the total and partial cross sections are expected to remain essentially unaffected if the dynamics calculations are extended to three dimensions. Photodissociation through this state mainly proceeds via resonant levels of the coupled antisymmetric−symmetric stretching motion. The vibrational substructure of the total absorption cross section in the bound and resonant region of excitation energies has been analyzed. An assignment has been suggested for the lines corresponding to bound vibrational levels and for the more pronounced resonance lines. Both the $2^2A''$ and the $3^2A'$ state absorb in essentially the same energy range between 7 and 8.5 eV. Hence the ratio of the integrated cross sections through both states corresponds to that of the photodissociation rates. Therefore it can be concluded that under interstellar conditions photodissociation of NH_2 through the $2^2A''$ state is much more

efficient than through the $3^2A'$ state. However, since the $2^2A''$ state has a $NH(a^1\Delta) + H$ asymptote, it does not contribute to the $NH(A^3\Pi) + H$ fragment fluorescence spectrum by Biehl et al.,[15] which has been compared to our results above.

For both the $2^2A''$ and the $3^2A''$ state, the geometry dependence of the transition dipole moments inside the Franck−Condon zone turns out to be important. In the case of the $2^2A''$ state it mainly influences the absolute numbers of the total and partial cross sections. In the case of the $3^2A''$ state, it affects both the shape and the absolute values of the total and partial cross sections. The nodal line in the dominant component of the transition dipole moment close to the ground state eq. geometry causes an intermediate minimum in the broad dissociation continuum feature. Due to the increase of the transition dipole moment with respect to the constant transition dipole moment by up to a factor of 4 at the boundary of the Franck−Condon region, the cross sections are considerably enhanced if the surface of the transition dipole moment is taken into account instead of using the relatively small constant transition dipole moment of 0.112 au at the ground state eq. geometry. Since direct photodissociation can occur through this state, the lower excitation energy range of the spectrum is particularly enhanced.

It is expected that the integrated total cross sections given in this work remain essentially unchanged in a full 3D photodissociation study. Since the initial vibrational wave function is normalized, discrepancies between those results from a 2D and a 3D calculation would only result from non-Franck−Condon effects related to the behavior of the dipole transition moments as function of the bending motion. Since the interstellar radiation field increases by a factor of about 1.5 in the range from 130 to 160 nm (i.e. from 9.54 to 7.75 eV),[29] the ratio of the photodissociation rates through the $3^2A'$ and the $3^2A''$ state correspond to about 1.5 × the ratio of the integrated cross sections of photodissociation through these states, i.e. $k_{\text{ph.d.}}^{3^2A'}/k_{\text{ph.d.}}^{3^2A''} \simeq 0.86$. The same consideration leads to a ratio of $k_{\text{ph.d.}}^{2^2A''}/k_{\text{ph.d.}}^{3^2A''} \simeq 7.62$. This comparison shows that photodissociation through the $2^2A''$ state is by far the most efficient fragmentation process of the molecule under interstellar conditions. By this result we hope to encourage experimentalists to record the fluorescence spectrum of the $NH(a^1\Delta)$ fragment of this state and to determine the branching ratio of the $NH(a^1\Delta)$ and $NH(A^3\Pi)$ fragments as a function of excitation energy.

Acknowledgment. The author is indebted to Dr. R. Vetter (University of Potsdam, Germany) for performing the ab initio electronic structure calculations. The computing facilities of the University of Leiden, The Netherlands, which have been used for carrying out this project, and the financial support of the project by the European Community in the framework of the program "Human capital and mobility" are greatfully acknowledged.

References and Notes

(1) Feldman, P. D.; Fournier, K. B.; Grinin, V. P.; Zverva, A. M. *Astrophys. J.* **1993**, *404*, 348.
(2) Jansen, D. J. Doctoral thesis, University of Leiden, 1995.
(3) Le Bourlot, J. *Astron. Astrophys.* **1991**, *242*, 235.
(4) Pineau des Forêt, G.; Roueff, E.; Schilke, P; Flower, D. R. *MNRAS* **1993**, *262*, 915.
(5) Tielens, A. G. G. M.; Hollenbach, D. J. *Astrophys. J.* **1985**, *291*, 722.
(6) Vetter, R.; Zülicke, L.; Koch, A.; Van Dishoeck, E. F.; Peyerimhoff, S. D. *J. Chem. Phys.* **1996**, *104*, 5558.
(7) Buenker, R. J.; Peyerimhoff, S. D. *Theor. Chim. Acta* **1974**, *35*, 33.
(8) Buenker, R. J.; Peyerimhoff, S. D. *Theor. Chim. Acta* **1975**, *39*, 217.
(9) Buenker, R. J., Peyerimhoff, S. D.; Butscher, W. *Mol. Phys.* **1978**, *35*, 771.
(10) Buenker, R. J.; Peyerimhoff, S. D.; Bruna, P. In *Computational Theoretical Organic Chemistry*; Csizmadia, I. G., Daudel, R., Eds.; Reidel: Dordrecht, 1980; p 55.
(11) Dressler, K.; Ramsay, D. A. *Philos. Trans. R. Soc. London Ser. A* **1959**, *251*, 553.
(12) Bell, S.; Schaefer, H. F., III. *J. Chem. Phys.* **1977**, *67*, 5173.
(13) Dunlavey, S. J.; Dyke, J. M.; Jonathan, N.; Morris, A. *Mol. Phys.* **1980**, *39*, 1121.
(14) Saxon, R. P.; Lengsfield, B. H., III; Liu, B. *J. Chem.Phys.* **1983**, *78*, 312.
(15) Biehl, H.; Schönnenbeck, G.; Stuhl, F. *J. Chem. Phys.* **1994**, *101*, 3819.
(16) Henriksen, N. E.; Zhang, J.; Imre, D. G. *J. Chem. Phys.* **1988**, *89*, 5607.
(17) Kenner, R. D.; Browarzik R. K.; Stuhl, F. *Chem. Phys.* **1988**, *121*, 457.
(18) Schinke, R. Photodissociation Dynamics Code.
(19) Bearda, R. A.; Kroes, G. J.; Van Hemert, M. C.; Van Dishoeck, E. F. *J. Chem. Phys.* **1993**, *100*, 1113.
(20) Balint-Kurti, G. G.; Dixon, R. N.; Marston, C. C. *J. Chem. Soc., Faraday Trans.* **1990**, *86*, 1741.
(21) Koch, A.; Van Hemert, M. C.; Van Dishoeck, E. F. *J. Chem. Phys.* **1995**, *103*, 7006.
(22) Koch, A. *Chem. Phys. Lett.* **1995**, *244*, 275.
(23) Schinke, R. *Photodissociation Dynamics*; Cambridge Monographs of Atomic, Molecular and Chemical Physics 1; Dalgarno, A., Knight, P. L., Read, F. H., Zare, R. N. Eds.; Cambridge University Press: Cambridge, 1993.
(24) Kroes, G. J. *J. Chem. Phys.* **1994**, *101*, 5792.
(25) Zhang, J.; Imre, D. G. *J. Chem. Phys.* **1989**, *90*, 1666.
(26) Kosloff, D.; Kosloff, R. *J. Comput. Phys.* **1983**, *52*, 35.
(27) Park, T. J.; Light, J. C. *J. Chem. Phys.* **1986**, *85*, 5870.
(28) McKellar, A. R. W.; Vervloet, M.; Burkholder, J. B.; Howard, C. J. *J. Mol. Spectrosc.* **1980**, *142*, 319.
(29) Draine, B. T. *Astrophys. J., Suppl. Ser*. **1987**, *36*, 595.